Supporting Information for

Tajik Basin and Southwestern Tian Shan, Northwestern India-Asia Collision Zone: 2. Timing of Basin Inversion, Tian Shan Mountain Building, and Relation to Pamir-Plateau Advance and Deep India-Asia Indentation

Sanaa Abdulhameed[1], Lothar Ratschbacher[1], Raymond Jonckheere[1], Łukasz Gągała[1,2], Eva Enkelmann[3], Alexandra Käßner[1], Myriam S. C. Kars[4], Adam Szulc[1,5], Sofia-Katerina Kufner[6], Bernd Schurr[6], Jean-Claude Ringenbach[7], Mykhaylo Nakapelyukh[1,8], Jahanzeb Khan[1,9], Mustafo Gadoev[10], and Ilhomjon Oimahmadov[10]

[1]Geologie, Technische Universität Bergakademie Freiberg, Freiberg, Germany, [2]Present address: Hellenic Petroleum, Marousi, Greece, [3]Department of Geoscience, University of Calgary, Alberta, Canada, [4]Center for Advanced Marine Core Research, Kochi University, Nankoku, Japan, [5]now at CASP, Cambridge, UK, [6]Deutsches GeoForschungsZentrum GFZ, Potsdam, Germany, [7] E2S-UPPA, CNRS, Univ. Pau & Pays Adour, Pau, France, [8]now at S. I. Subbotin Institute of Geophysics, NAS of Ukraine, Kyiv, Ukraine, [9]now at Geology, Azad Jammu and Kashmir University, Muzaffarabad, Pakistan, [10]Institute of Geology, Earthquake Engineering and Seismology, Tajik Academy of Sciences, Dushanbe, Tajikistan

Contents of this File

Introduction

Supporting information S1 summarizes the Soviet-time geologic maps, describes the experimental aspects of our apatite fission-track (AFT) dating and thermal-history modeling, and the apatite and zircon (U, Th)/He (AHe, ZHe) dating, respectively. Table S1 provides the vitrinite-reflectance maturity data, Table S2 the AFT data, and Table S3 the AHe and ZHe data. In Table S3, we assess the grain ages, identify outliers, and show, which grains were included in the mean ZHe and AHe age calculations.

Figure S1 compiles the stratigraphic columns of the Tajik basin and Uzbek Gissar. Figure S2 shows radial plots of the single-grain AFT ages. Figure S3 plots the single-grain AHe ages against equivalent uranium concentration (eU) and grain width. Figure S4 provides the AFT track-length distributions and the temperature-time modeling solutions. Dataset S1 provides in Tables S4–S6 sample information and partly recalculated ages from the work of Chapman et al. (2017) and Jepson et al. (2018a,b).

Supporting information S1

Soviet-time Geologic maps

The base for our maps and the geologic and structural interpretations are the Soviet-time geological maps of the USSR at a scale of 1:200,000. They were issued by the Russian Geological Research Institute (GRI), Nedra, Moscow, in Russian. In the text, we reference the sheets that were used for map construction as GRI (1961-1964). In detail these include:

Burmakin, A.V., Starshinin, D. A., & Likhachev, V. I (1961). *Geological map of the USSR of 1: 200 000 scales, Sheet J-42-XI*, Russ. Geol. Res. Inst., Nedra, Moscow.

Lyoskind, S. Y., Novikova, L. A., & Yakusheva V.M. (1963). *Geological map of the USSR of 1: 200 000 scales, Sheet J-42-XV*, Russ. Geol. Res. Inst., Nedra, Moscow.

Lyoskind, S. Y., Novikova, L. A., & Dolgonos, L. G. (1963). *Geological map of the USSR of 1: 200 000 scales, Sheet J-42-XVII*, Russ. Geol. Res. Inst., Nedra, Moscow.

Lyoskind, S. Y., Novikova, L. A., & Yakusheva, V. M. (1964). *Geological map of the USSR of 1: 200 000 scales, Sheet J-42-XVI*, Russ. Geol. Res. Inst., Nedra, Moscow.

Rubanov, D. A., Puniklenko, I. A., Rubanov, A. A., & Alfyorov, G. Y. (1963). *Geological map of the USSR of 1: 200 000 scales, Sheet J-42-XIV*, Russ. Geol. Res. Inst., Nedra, Moscow.

We cited the sheets, when extracting specific information.

Sample Preparation, Apatite Fission-Track Dating, and Modeling Aspects, Track-laboratory TU Bergakademie Freiberg

Samples were crushed with a mechanical crusher into cm-sized pieces, fragmented by high-voltage mineral liberation (SELFRAG®) (Sperner et al., 2014), and sieved to separate the 80–250 μm grain-size fraction. This fraction underwent further mineral purification by magnetic and heavy-liquid separation and handpicking. The apatite grains were mounted in epoxy resin, ground, and polished to expose internal surfaces. The mounts were etched in 5.5 M HNO_3 at 21°C for 20 seconds (Carlson, 1999). After etching, the mounts were covered with 1 cm^2 muscovite external detectors (Gleadow, 1981; Hurford and Green, 1982), and stacked with three to four age-standard mounts (Durango apatite, 31.4 ± 0.5 Ma, 2σ, Hurford, 1991) and standard uranium glass (IRMM-450R) in irradiation containers for age determination with the ζ method (Hurford and Green, 1982, 1983). The samples were irradiated with a thermal neutron fluence of 2.5×10^{15} cm^{-2} in channel X26 of the BR1 reactor (Mol, Belgium). Following neutron irradiation, the external detectors were detached and etched in 48% HF solution for 30 minutes at room temperature to expose the induced tracks. They were repositioned track-side down on the apatite mounts for track counting (Jonckheere et al., 2003). Apatite grains were counted at 500-times magnification.

A second apatite mount was prepared for confined track-length measurements. These mounts were irradiated at 30° from normal incidence with 10^6 cm^{-2} 11.1 MeV/amu ^{132}Xe-ions from the UNILAC linear accelerator at the Helmholtzzentrum für Schwerionenforschung (Darmstadt, Germany). This increases the number of measureable confined tracks (TinT's) (Jonckheere et al., 2007; Min et al., 2007). After irradiation, the length mounts were etched in 5.5 M HNO$_3$ at 21°C for 20 seconds (Carlson et al., 1999) to be consistent with the annealing model of Ketcham et al. (1999, 2007). The temperature-time (T-t) history of samples with >33 measured confined tracks were modeled with HeFTy (Ketcham, 2005). Our modeling aimed at determining data-driven solutions, i.e., at finding T-t paths consistent with the AFT data, with minimal bias by deliberate or inadvertent constraints. To this end, we set three identical overlapping box constraints (10–140°C; 0–1.5 or 2 × t_{FT}; t_{FT} = AFT age) plus the fixed bar constraint at 0 Ma. Segments joining the nodes were 'monotonic variable', allowing heating or cooling. 'Monotonic consistent' segments, which limit the set of T-t solutions to either pure monotonic cooling or heating histories, i.e., to a subset of the data-based solutions, are justifiable on the basis of compelling independent evidence, which was unavailable. No maximum heating or cooling rate was set to avoid biasing the estimate of the onset of a late cooling. The segments between nodes were halved once, allowing a measure of non-linear heating or cooling between nodes, providing T-t paths with some detail without slowing down the calculations too much. The initial mean track length was set to the operator's (S.A.) value for induced tracks (15.95 µm) determined from measurements of length standards to allow for personal length-measurement criteria (Ketcham et al., 2015). We selected the curvilinear model that best fits the lab annealing data for our etching conditions (Ketcham et al., 1999). We used the default kinetic-parameter setting because no other value was determined. *c*-axis projection was not modeled, because we found that none of the projection models eliminated the anisotropy of the measured lengths (Käßner et al., 2016). The modeling was continued until 500 'good-fit' solutions had been found, using the Kolmogorov-Smirnov criterion with default cut-offs for good (α = 0.05) and acceptable (α = 0.5) fits. Our approach aimed at finding a broad range of data-driven solutions with minimal risk of introducing artifacts. For the purpose of interpretation, the modeling solutions are presented in different forms: (1) the set of good-fit T–t solutions; (2) contours of the node densities of 500 good-fit T–t paths.

Apatite and Zircon (U, Th)/He Dating, Universität Tübingen

For AHe and ZHe dating, clear idiomorphic grains without inclusions, impurities, or cracks were picked, and the grain dimensions were measured for calculating the α-correction factors (Farley et al., 1996). Each grain was packed in niobium tubes. We analyzed 2–5 aliquots per sample in the Patterson He-extraction line at the Universität Tübingen, Germany, equipped with a 960 nm diode laser and a quadrupole mass spectrometer. The grains were heated for 5 minutes at ~1100 °C to extract the He. Each grain was re-heated and re-analyzed to confirm complete degassing in the first step; the re-extracts always amounted to <1% of the initial signal. We sent the grain packages to the University of Arizona at Tucson for ICPMS measurement of U, Th, and Sm (Reiners and Nicolescu, 2006). Whereas the propagated analytical uncertainties for igneous samples lead to an estimated analytical uncertainty on the (U, Th)/He ages of ~1–3 % (1σ), the reproducibility of repeat analyses of (U,Th)/He ages is significantly worse than the analytical precision. Ages typically show excess scatter, with a standard deviation of at least 5%, and in many cases more than 10%. We report the unweighted arithmetic mean and standard error of the grain ages as the AHe and ZHe ages and their uncertainties. Fragments of the Durango apatite and Fish Canyon zircon age standards, analyzed along with the unknowns, yielded

consistent results with an average value of 31.6 ± 0.3 Ma and 30.1 ± 0.6 Ma, respectively. Based on the He, U, Th, Sm measurements, the single grain parameters (length, width, volume), and the effective uranium concentrations (eU; Figure S3), Table S3 identifies outliers and lists which grains were excluded from the mean AHe age calculations.

Tables S1 to S3 are provided as separate files

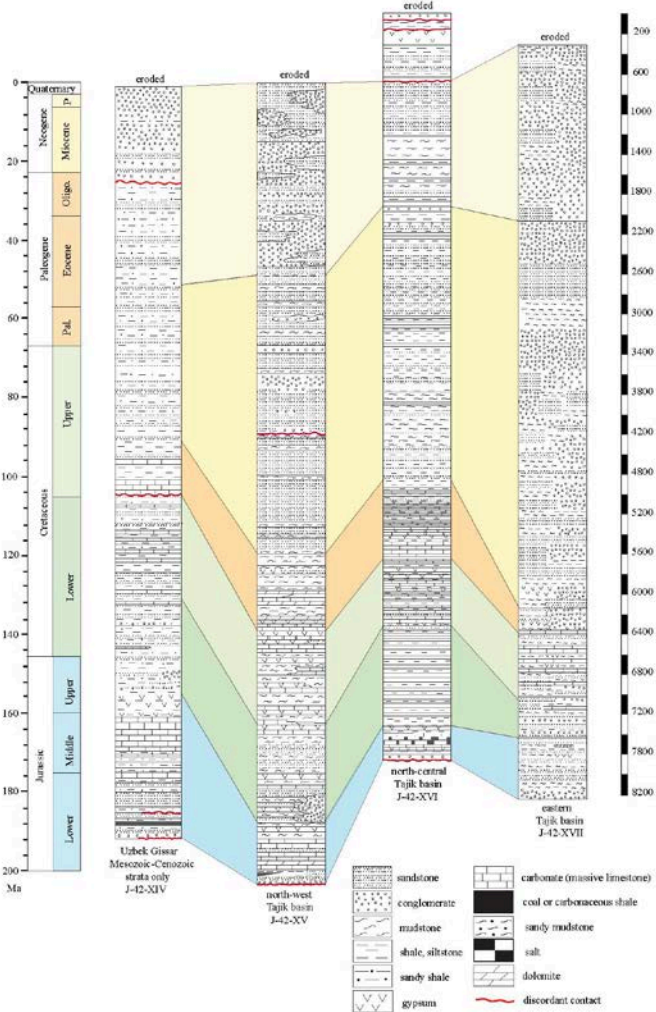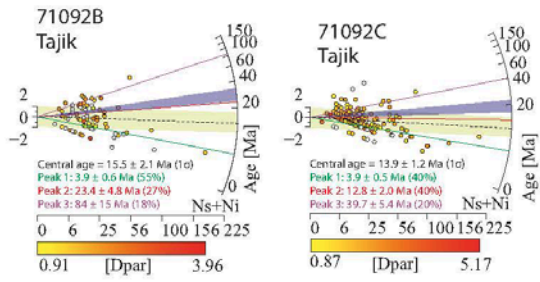**Dataset S1 with Tables S4 to Table S6 is provided as a separate file**

Figures S1-S4

Figure S1. Stratigraphic columns for the Tajik basin and Uzbek Gissar arranged from west, i.e., the Uzbek Gissar, to the east across the Tajik basin, highlighting the thickness changes of the strata. Modified from Rubanov et al. (1963), Lyoskind et al. (1963a,b, 1964), and Vlasov et al. (2001); sheet numbers are given at the bottom of the columns.
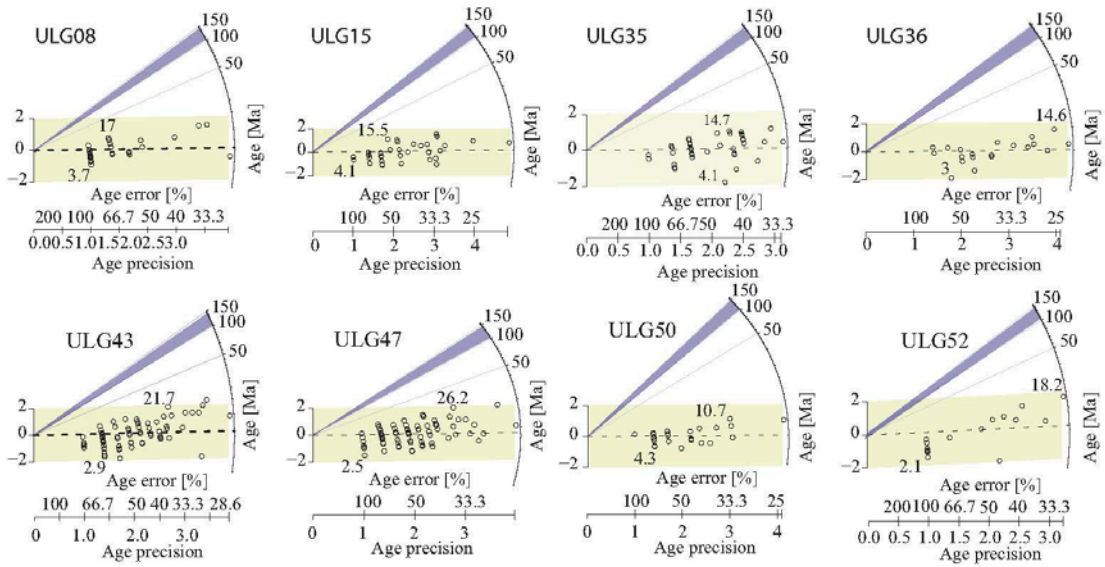
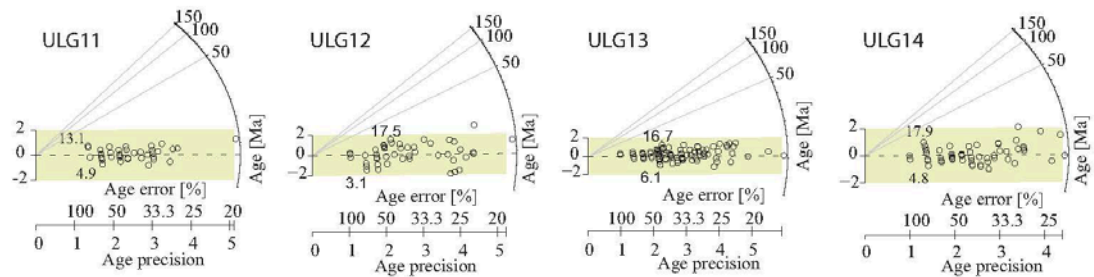# Sedimentary rocks of the Tajik basin and the Hakimi basin, Tajik Gissar
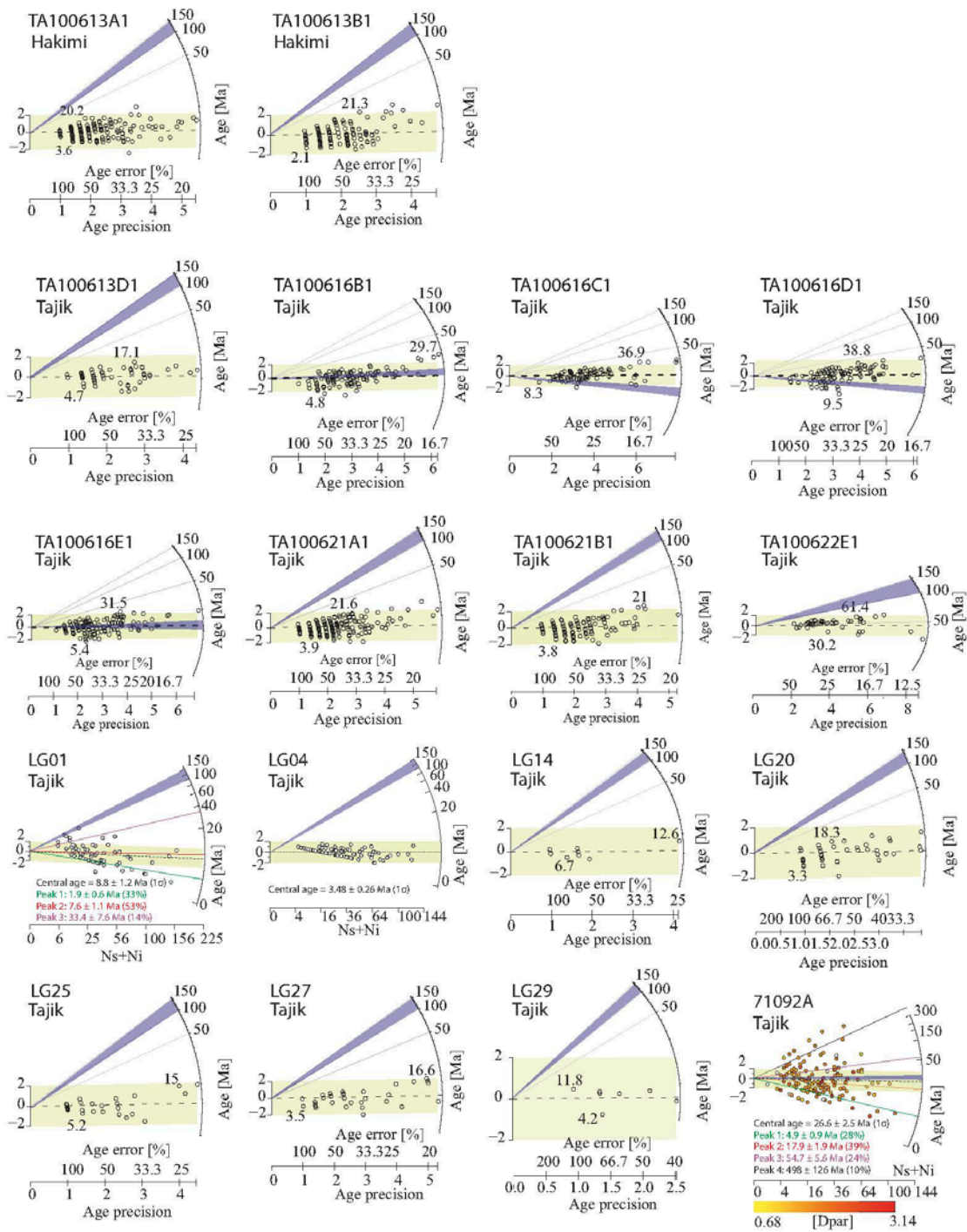
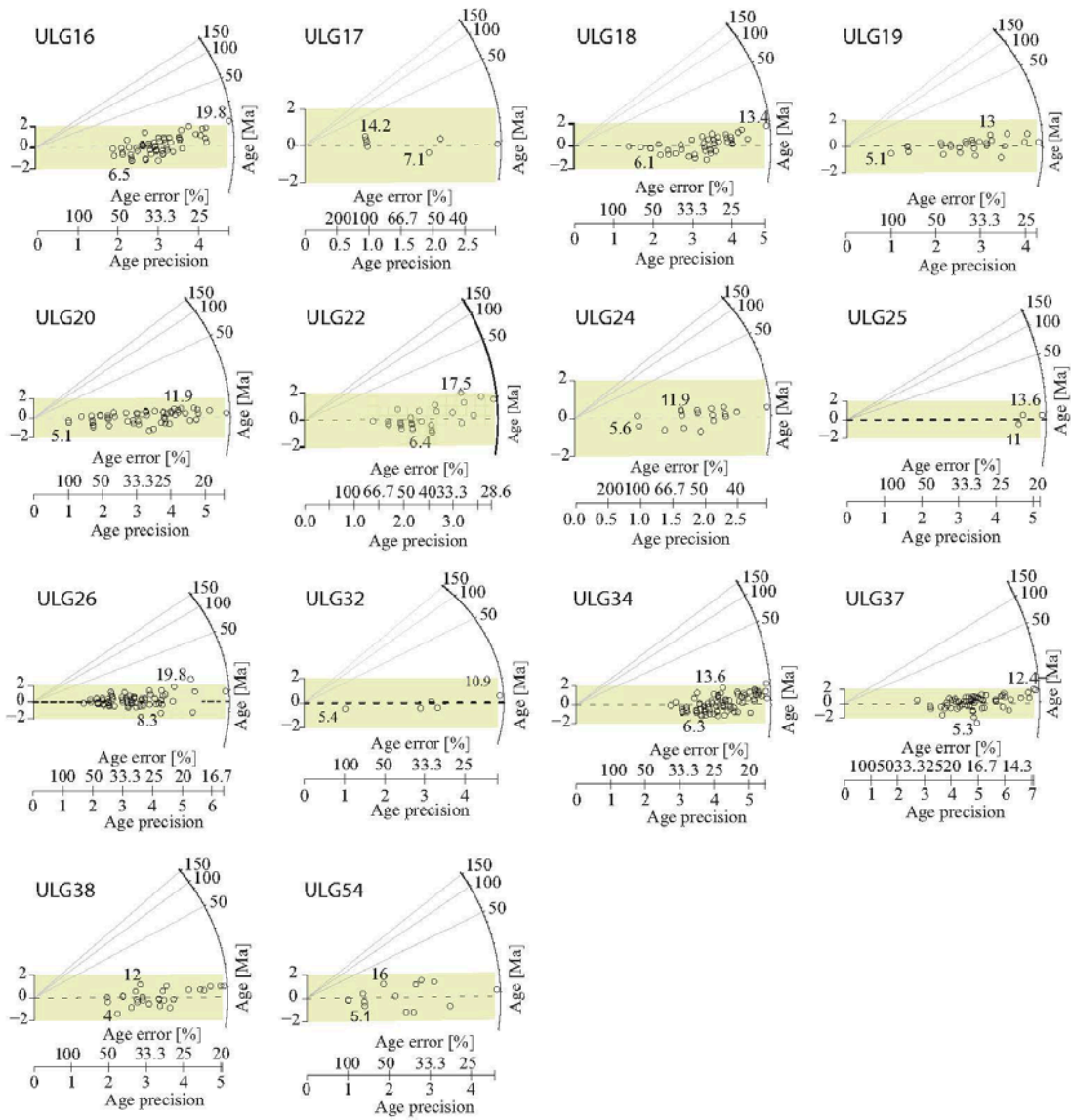# Sedimentary rocks of the Tajik basin and the Hakimi basin, Tajik Gissar, continuation

71092B
Tajik

Central age = 15.5 ± 2.1 Ma (1σ)
Peak 1: 3.9 ± 0.6 Ma (55%)
Peak 2: 23.4 ± 4.8 Ma (27%)
Peak 3: 84 ± 15 Ma (18%)

71092C
Tajik

Central age = 13.9 ± 1.2 Ma (1σ)
Peak 1: 3.9 ± 0.5 Ma (40%)
Peak 2: 12.8 ± 2.0 Ma (40%)
Peak 3: 39.7 ± 5.4 Ma (20%)

Sedimentary rock cover of the Uzbek Gissar

ULG08   ULG15   ULG35   ULG36

ULG43   ULG47   ULG50   ULG52

Crystalline basement rocks of the Uzbek Gissar

ULG11   ULG12   ULG13   ULG14

Crystalline basement rocks of the Uzbek Gissar

Crystalline rocks of the basement spur at the western edge of the southwestern Tian Shan
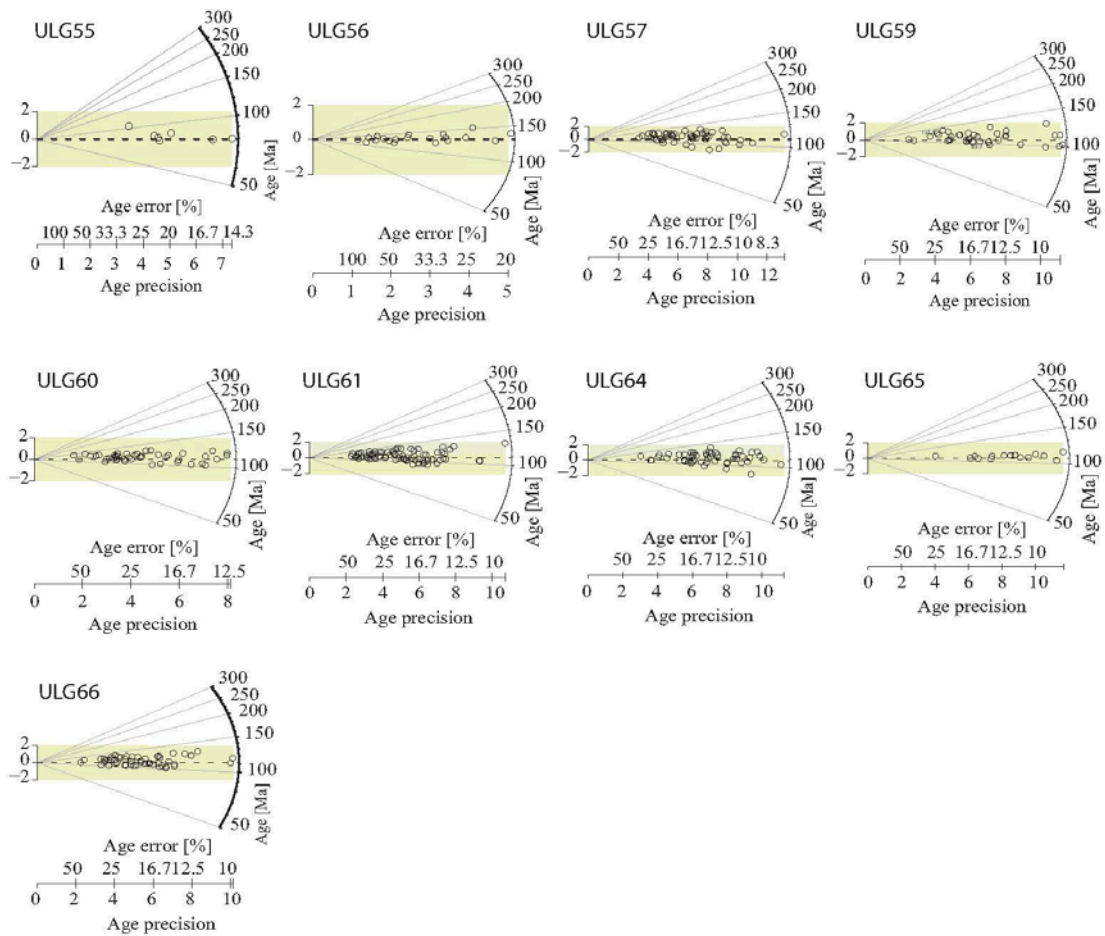

Figure S2. Radial plots (Galbraith 1990; equations 2 and 6) of the single-grain apatite fission-track ages. Blue sectors bracket the stratigraphic age of the samples from the Lower Cretaceous and Oligocene-Neogene strata. Light-green bands highlight the dispersion of the single-grain ages within the ±2σ scatter. Numbers inside the plots give the minimum and maximum single-grain ages. For a few plots with dispersed single-grain dates, we show the central age together with age peaks calculated with DensityPlotter (Vermeesch, 2012).
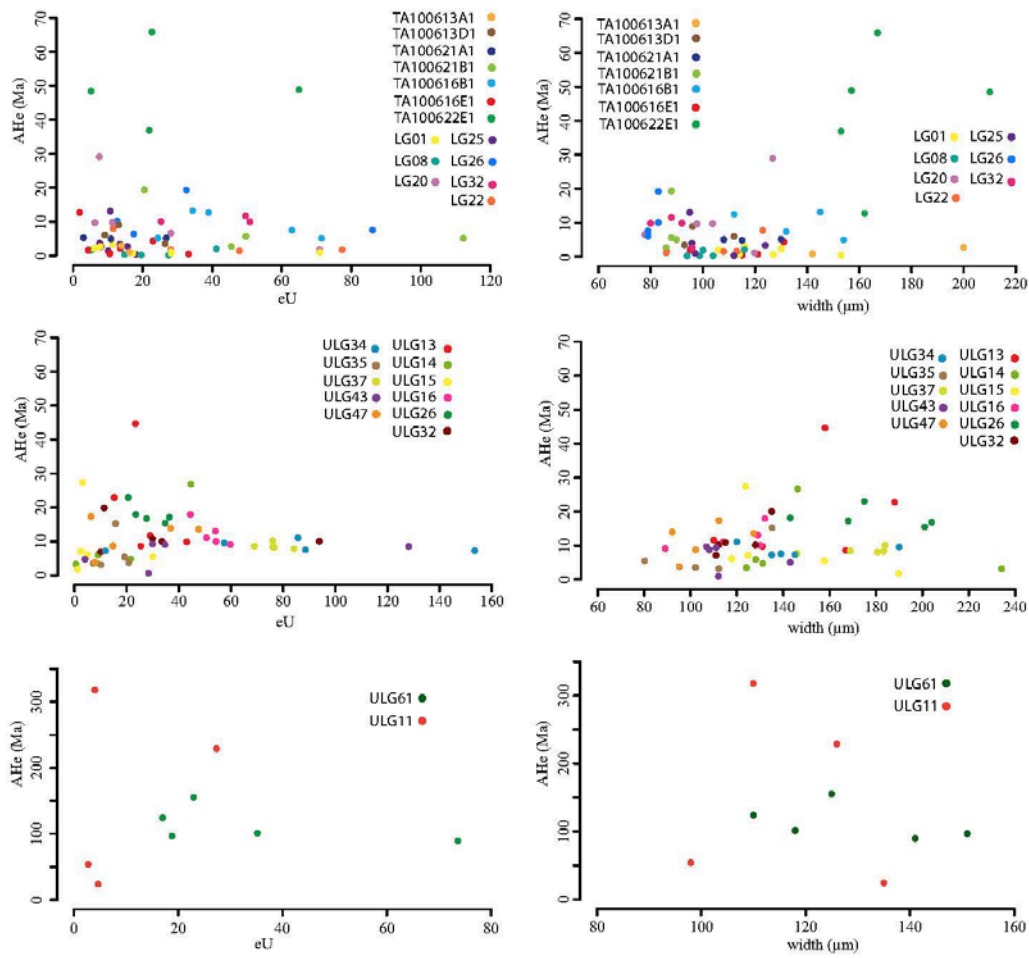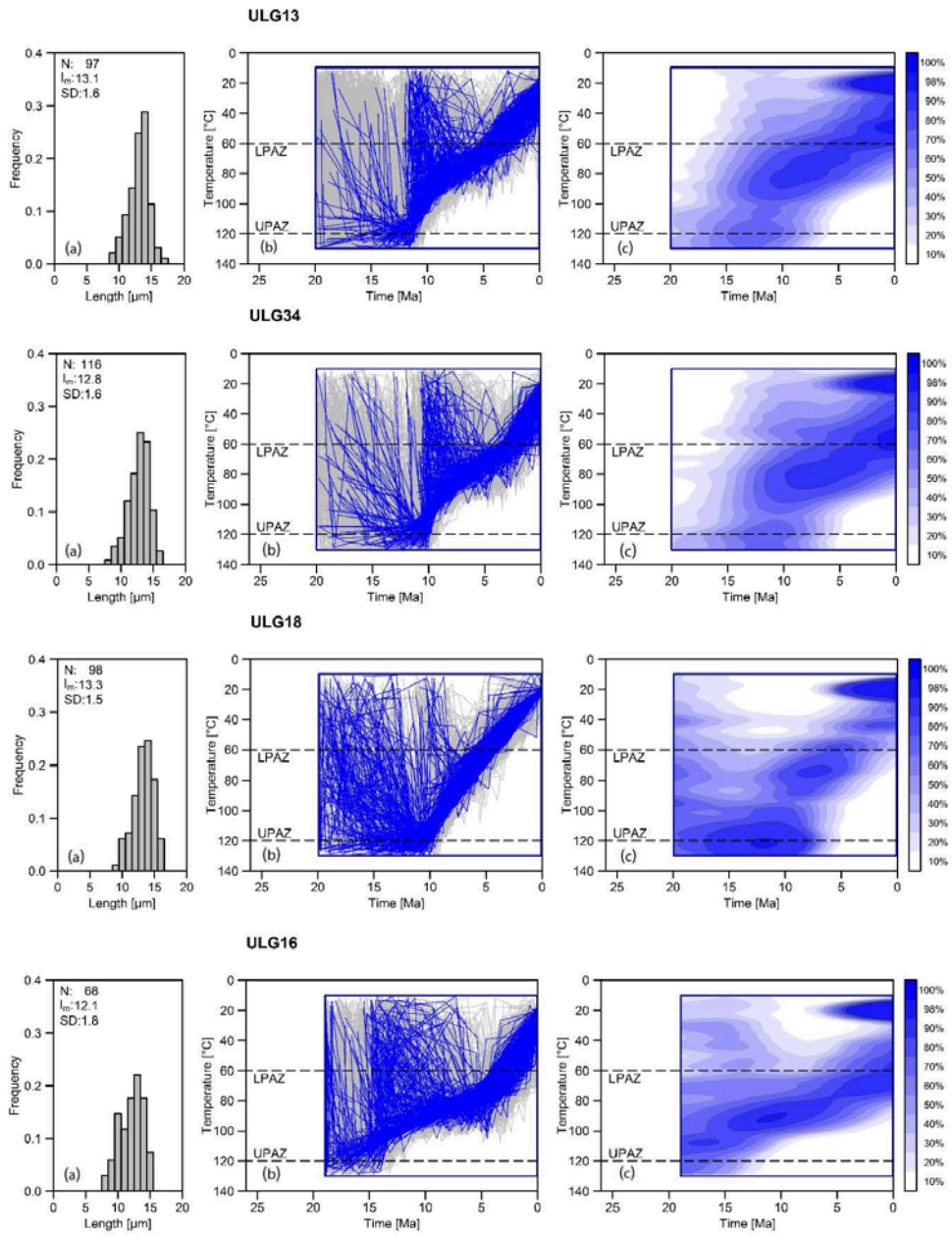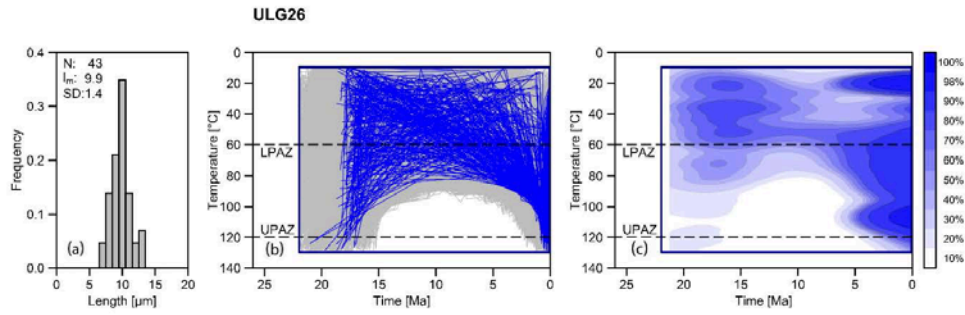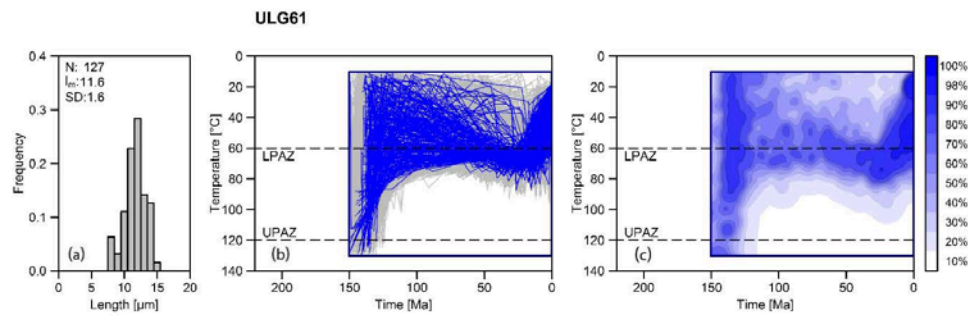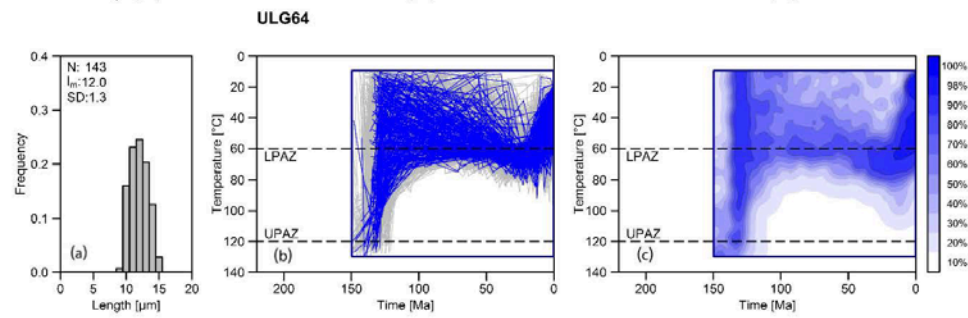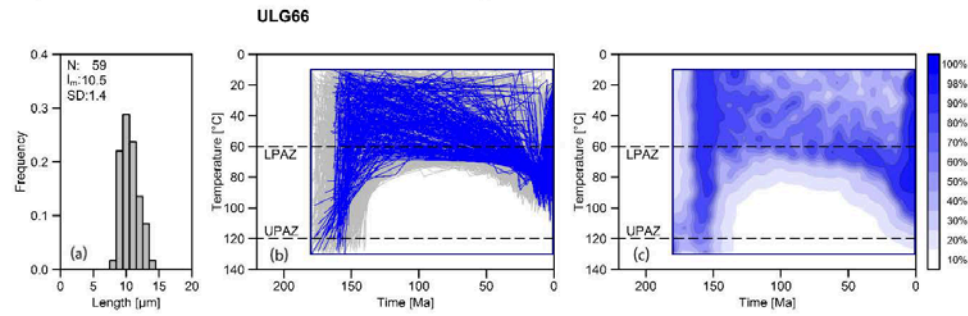
Figure S3. Single-grain apatite (U, Th)/He (AHe) ages plotted against equivalent uranium concentration (eU) and grain width, based on data listed in Table S3. Data in Figure S3 and Table S3 were used for identifying outliers, which were not included in the sample-age calculations (marked bold in Table S3).

Crystalline basement rocks of the Uzbek Gissar

ULG13

ULG34

ULG18

ULG16

ULG26

Crystalline rocks of the basement spur at the western edge of the southwestern Tian Shan
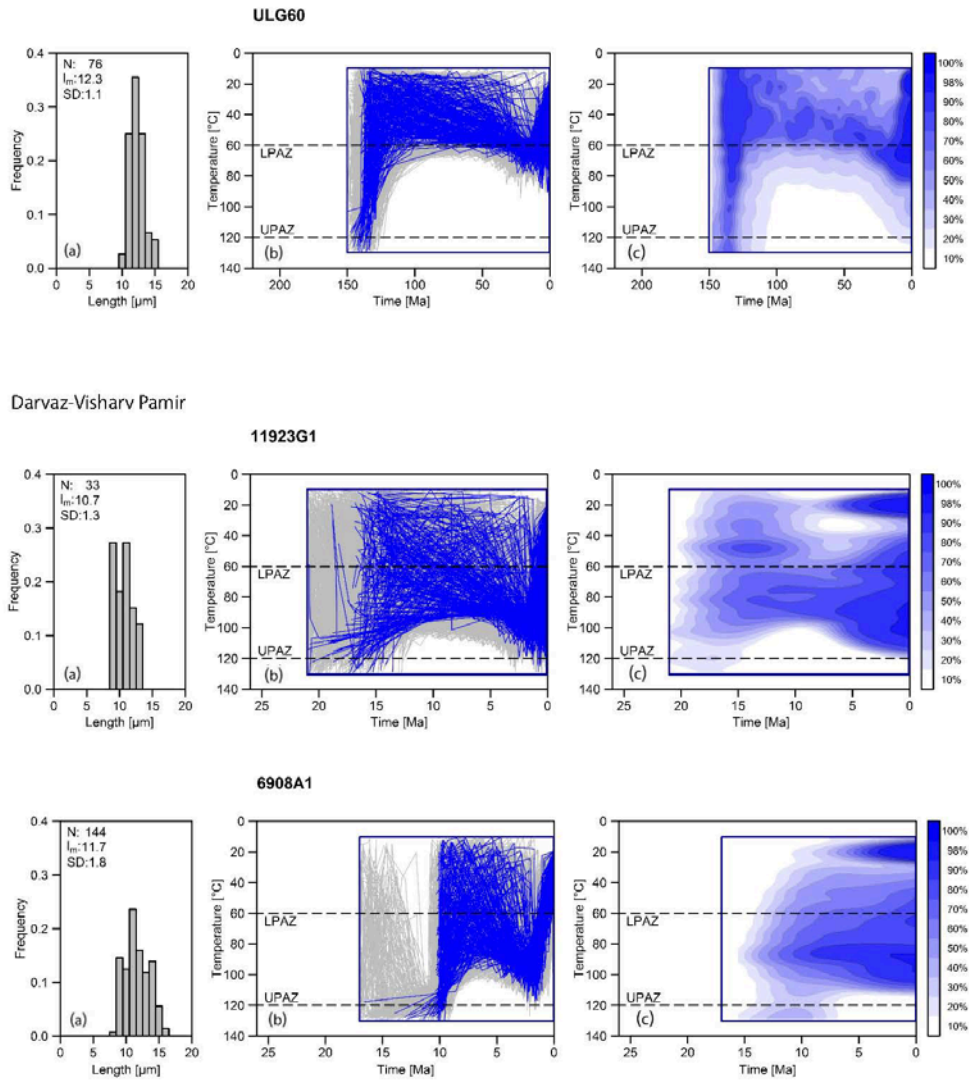
ULG66

ULG64

ULG61

Figure S4. Results of thermal modeling with HeFTy (Ketcham, 2005) based on apatite fission-track age and confined track-length data. Left: confined track-length distributions. Middle: acceptable- (gray) and good-fit (blue) paths; computation was stopped at 500 good-fit paths but only the first block of 250 single good-fit path is shown. Right: node density contours of 500 good-fit paths. Blue color scale legend indicates percentage node densities. LPAZ, lower apatite partial-annealing-zone boundary. UPAZ, upper apatite partial-annealing-zone boundary. Blue-edged rectangles indicate user-defined box constraints.

References

Carlson, W.D., Donelick, R.A., & Ketcham, R.A. (1999). Variability of apatite fission-track annealing kinetics: I. Experimental results. *American Mineralogist, 84*, 1213–1223.

Chapman, J. B., Carrapa, B., Ballato, P., DeCelles, P.G., Worthington, J., Oimahmadov, I., Gadoev, M., & Ketcham, R. (2017). Intracontinental subduction beneath the Pamir Mountains: Constraints from thermokinematic modeling of shortening in the Tajik fold-and-thrust belt. *Geol. Soc. Amer. Bulletin, 129*, 1450–1471. doi:10.1130/B31730.1

Farley, K. A., Wolf, R. A., & Silver, L. T. (1996). The effects of long alpha-stopping distances on U-Th/He dates. *Geochimica et Cosmochimica Acta, 60*, 4223–4230.

Galbraith, R. F. (1990). The radial plot: Graphical assessment of spread in ages. *Nucl. Tracks Radiat. Meas., 17*, 207–214. doi:10.1016/1359-0189(90)90036-W

Gleadow, A. J. W. (1981). Fission-track dating methods: What are the real alternatives? *Nuclear Tracks, 5*, 3–14.

Hurford, A. J. (1991). Fission track dating. In P. L. Smart & P. D. Frances (Eds.). *Quaternary dating methods; a user's guide*. Quaternary Research Association Technical Guide, 4, 84–107.

Hurford, A. J., & Green, P. F. (1982). A user's guide to fission track dating calibration. *Earth and Planetary Science Letters, 50*, 343–354.

Hurford, A. J., & Green, P. F. (1983). The zeta age calibration of fission track dating. *Isotope Geoscience, 1*, 285–317.

Jepson, G., Glorie, S., Konopelko, D., Gillespie, J., Danišık, M., Evans, N. J., Mamadjanov, Y., & Collins, A.S. (2018a). Thermochronological insights into the structural contact between the Tian Shan and Pamirs, Tajikistan. *Terra Nova. 30*, 95–104. https://doi.org/10.1111/ter.12313

Jepson, G., Glorie, S., Konopelko, D., Mirkamalov, R., Danišík, M., & Collins, A. S. (2018b). The low-temperature thermo-tectonic evolution of the western Tian Shan, Uzbekistan. *Gondwana Research, 64*, 122–136. https://doi.org/10.1016/j.gr.2018.08.003

Jonckheere R., Ratschbacher, L., & Wagner, G. A. (2003). A repositioning technique for counting induced fission-tracks in muscovite external detectors in single-grain dating of minerals with low and inhomogeneous uranium concentrations. *Radiation Measurements, 37*, 217–219. doi:10.1016/s1350-4487(03)00029-5

Jonckheere, R., Enkelmann, E., Min, M., Trautmann, C., & Ratschbacher, L. (2007). Confined fission tracks in ion-irradiated and step-etched prismatic sections of Durango apatite. *Chemical Geology, 242*, 202–217. doi:10.1016/j.chemgeo.2007.03.015

Käßner, A., L. Ratschbacher, R. Jonckheere, E. Enkelmann, J. Khan, B.-L. Sonntag, R. Gloaguen, M. Gadoev, & I. Oimahmadov (2016). Cenozoic intracontinental deformation and exhumation at the northwestern tip of the India-Asia collision– southwestern Tian Shan, Tajikistan, and Kyrgyzstan. *Tectonics, 35*, 2171–2194. doi:10.1002/2015TC003897

Ketcham, R. A. (2005). Forward and inverse modeling of low-temperature thermochronometry data In P. W. Reiners & T. A. Ehlers (Eds.). *Low Temperature Thermochronology: Techniques, Interpretations and Applications*. Reviews in Mineralogy and Geochemistry, 58, 275–314. doi:10.2138/rmg.2005.58.11

Ketcham, R. A., Donelick, R. A., & Carlson, W. D. (1999). Variability of apatite fission-track annealing kinetics: III. Extrapolation to geological time scales. *American Mineralogist, 84*, 1235–1255.

Ketcham, R. A., Carter, A., Donelick, R. A., Barbarand, J., & Hurford, A. J. (2007). Improved measurement of fission-track annealing in apatite using c-axis projection. *American Mineralogists, 92*, 789–798. doi:10.2138/am.2007.2280

Ketcham, R. A., Carter, A., & Hurford A. J. (2015). Inter-laboratory comparison of fission track confined length and etch figure measurements in apatite. *American Mineralogist, 100*, 1452–1468.

Lyoskind, S. Y., Novikova, L. A., & Dolgonos, L. G. (1963b). *Geological map of the USSR of 1: 200 000 scales, Sheet J-42-XVII*, Russ. Geol. Res. Inst., Nedra, Moscow.

Lyoskind, S. Y., Novikova, L. A., & Yakusheva, V. M. (1964). *Geological map of the USSR of 1: 200 000 scales, Sheet J-42-XVI*, Russ. Geol. Res. Inst., Nedra, Moscow.

Min, M., Enkelmann, E., Jonckheere, R., Trautmann, C., & Ratschbacher, L. (2007). Measurements of fossil confined fission tracks in ion-irradiated apatite samples with low track densities. *Nuclear Instruments and Methods in Physic Research B, 259*, 943–950. doi:10.1016/j.nimb.2007.03.012

Reiners, P. W.; & Nicolescu. S. (2006). Measurement of parent nuclides for (U-Th)/He chronometry by solution sector ICP-MS, *ARHDL Report 1*, www.geo.arizona.edu/~reiners/arhdl/arhdl.htm.

Rubanov, D. A., Puniklenko, I. A., Rubanov, A. A., & Alfyorov, G. Y. (1963). *Geological map of the USSR of 1: 200 000 scales, Sheet J-42-XIV*, Russ. Geol. Res. Inst., Nedra, Moscow.

Sperner, B., Jonckheere, R., & Pfänder, J. A. (2014). Testing the influence of high-voltage mineral liberation on grain size, shape and yield, and on fission track and ^{40}Ar/^{39}Ar dating. *Chemical Geology, 371*, 83–95. doi: 10.1016/j.chemgeo.2014.02.003

Vermeesch, P. (2012). On the visualization of detrital age distributions. *Chemical Geology, 312-313*, 190–194. doi: 10.1016/j.chemgeo.2012.04.021

Vlasov, N. G., Dyakov, Y. A., & Cherev, E. S. (1991). *Geological map of the Tajik SSR and adjacent territories, 1:500,000*, Vsesojuznoi Geol. Inst. Leningrad, Saint Petersburg.